Pergamon

PII: S1359-6454(96)00399-0

Acta mater. Vol. 45, No. 7, pp. 2735–2746, 1997

Published by Elsevier Science Ltd

1359-6454/97 $17.00 + 0.00

DEPENDENCE OF CREEP FRACTURE OF INCONEL 718 ON GRAIN BOUNDARY PRECIPITATES

W. CHEN and M. C. CHATURVEDI

Department of Mechanical and Industrial Engineering, The University of Manitoba, Winnipeg, Manitoba, R3T 5V6 Canada

(Received 30 November 1995; accepted 12 November 1996)

Abstract—In this study, Inconel 718 was heat treated to obtain various materials with identical grain size and microstructures but with a different state of dispersion of δ precipitates at the GBs. The density of δ precipitates ρ in different materials was from 0% to about 70%. Creep tests were conducted on these materials at 795 MPa and 625°C. It was found that both the rupture time and total creep strain decreased with an increase in the value of ρ when its value was below about 45%. However, when the value of ρ was above 45%, both the rupture time and creep strain increased with an increase in ρ to a value much higher than that observed in the material without δ precipitates at GBs. SEM observations of the crept samples and their fracture surfaces showed that the presence of δ precipitates at GBs resulted in the formation of creep voids in all specimens. However, the effect of creep voids on the final fracture of the material was dependent upon the value of ρ. At lower values of ρ, creep voids were observed to be isolated, and the fracture may be due to the propagation of wedge cracks initiated at triple points of grain boundaries. At higher values of ρ, the probability of wedge crack formation might be reduced. The fracture would then be controlled by the growth of cavities coupled with grain boundary sliding, which was observed to be strongly influenced by precipitates at grain boundaries. ©*1997 Acta Metallurgica Inc.*

1. INTRODUCTION

During high temperature creep, the effect of precipitate particles at grain boundaries on the creep fracture is believed to depend not only upon the creep deformation conditions but also on the size of the particles [1, 2]. When the size is either very small (less than 100 nm), or very large (>50 μm) strengthening through the precipitates can be achieved either by their interaction with dislocations or by load transfer. When the size is between the extremes, creep voids are normally associated with the precipitates and detract from strengthening of the grain boundaries. As a result, since it is difficult for most engineering materials to have grain boundary precipitates with a size beyond the intermediate size range, it is generally believed that the presence of precipitates is detrimental to the creep fracture properties of a material. This also holds true for Inconel 718 in which precipitates of δ phase, which is orthorhombic Ni_3Nb, are normally present at grain boundaries [3]. The presence of δ precipitates at grain boundaries (GBs) in Inconel 718, though generally believed to be detrimental to the fracture properties of the material [3], has also been reported to be beneficial in enhancing its ductility and toughness [4, 5]. The δ precipitates at GBs are normally produced by a modification of the heat treatment procedures. These modified treatments may also significantly alter the state of distribution of strengthening γ'' precipitates within the grain material at the same time. As a result, the actual effect of these δ particles at GBs on the mechanical properties of the alloy may be complex and the analysis may not be as straight forward as has been assumed.

To study the effect of precipitates at grain boundaries on the creep fracture behavior, many research projects have been conducted to obtain an understanding of the mechanism of precipitate-induced void formation, and their growth and propagation [6]. In contrast to this, little information is available on the effect of the density of grain boundary particles on the creep fracture behavior. Such a study is important because it is believed that the variation in the precipitate density at grain boundaries may be able to change the sliding conditions along the boundaries resulting in possible beneficial influences on fracture behavior.

Previous studies have shown that the creep behavior of Inconel 718 is strongly dependent on the microstructure of grain boundaries [7, 8]. That is, the steady-state creep rate was observed to be independent of the strength of grain materials [7], and the stress dependence of the material was also observed to change by the decoration of δ precipitates at grain boundaries [8]. In the present study, Inconel 718 was heat treated to obtain various materials with identicial grain size and microstructures but with a different state of dispersion of δ precipitates at the GBs. Creep tests were then conducted on these materials to study the effect of the density of δ

Table 1. Chemical composition of Inconel 718 (wt %)

0.03/C	19.24/Fe	52.37/Ni	18.24/Cr	0.52/Al	0.97/Ti
3.07/Mo	4.98/(Nb + Ta)	0.007/Mn	0.007/S	0.30/Si	0.04/Cu

Table 2. Heat treatment procedures for Inconel 718

Material	Solution treatment	Aging treatment
Clean GBs	1020°C × 4 h (A.C.)	725°C × 25 h
δ precipitates at GBs	1020°C × 4 h (F.C.) + 900–1000°C for 1 h	725°C × 25 h

precipitates at grain boundaries on creep fracture behavior.

2. EXPERIMENTAL METHODS

The chemical composition of Inconel 718 used in this study, as determined by Arrow Lab, Wichita, Kansas (U.S.A.), is given in Table 1. A 2.54 mm thick sheet of the alloy was cold-rolled to a thickness of 1.4 mm and machined into flat samples with a gauge dimension of 1.3 mm × 5.3 mm × 25.4 mm. The creep samples were heat treated in accordance with the scheme illustrated in Table 2 (based on the work of other investigators [5, 6]), in order to obtain controlled and specific microstructures. The procedure was described in detail in an earlier communication [7, 8]. The heat-treated as well as creep-deformed specimens were examined using a JEOL 840 Analytical Scanning Electron Microscope and a JEOL 2000FX Analytical TEM/STEM. The size and number of precipitates at the grain boundaries were analyzed based on the binary images created from the secondary electron image of the precipitates. Such analysis was carried out continuously on the entire grain boundaries of several grains. The total length of the grain boundaries being analyzed was also measured on the SEM micrographs, and the average line density of precipitates at grain boundaries was then calculated based on the number and average size of precipitates on a given length of grain boundaries. More than 1000 particles on grain boundaries of at least five grains were scanned on each material. The creep tests were carried out at a temperature of 625°C and an applied stress of 795 MPa using Denison constant stress creep machines. The test temperature was controlled within $\pm$ 3°C and a flow of argon gas through the test chamber was maintained. Creep strain was recorded by a strip chart recorder.

3. RESULTS

3.1. Microstructures

The microstructures of the specimens that were furnace and air cooled from solid solution treatment at 1020°C are presented in Figs 1(a) and (b), respectively. It is seen that in contrast to the air-cooled material, which is free of any precipitates except for a few primary carbides, the furnace cooling produced coarse precipitates of $\gamma' + \gamma''$ phases within the grain interiors and small particles of δ phase at the grain boundaries. The furnace cooled material was given a partial solid solution treatment at temperatures in the range of 900°C–1000°C to dissolve the intra-granular precipitates but preserve those present at grain boundaries. As shown in Fig. 2(a), the partial solution treatment at 900°C was not successful in achieving this. However, when the temperature was 925°C or above, the specimens were free of all intra-granular precipitates and the δ precipitates at grain boundaries grew slightly compared to those observed before the partial solid solution treatment [Figs 2(b)–(d)].

The precipitates at grain boundaries were quantitatively examined by SEM. The results are shown in Fig. 3 where the average diameter and the line density of the precipitates have been plotted against the partial solid solution treatment temperature. It is seen that the average diameter of δ particles varies from 0.52 μm at 925°C to 0.34 μm at 975°C and the density from 67% at 925°C to 22% at 1000°C.

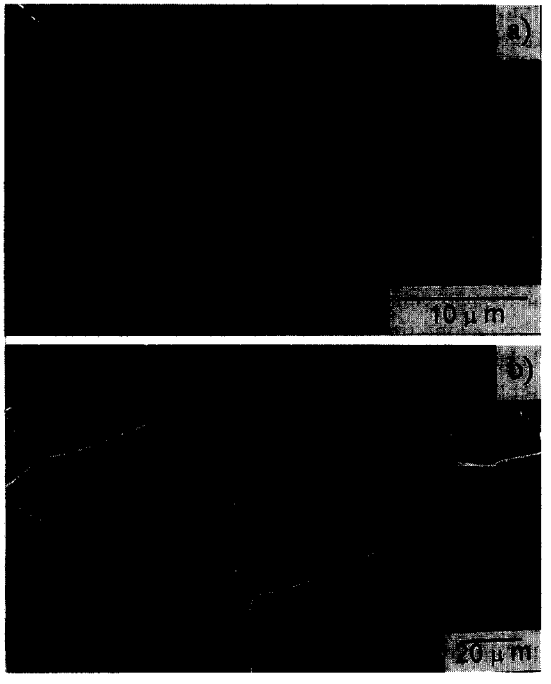

Fig. 1. SEM micrographs showing microstructures of the material (a) furnace-cooled from solid solution treatment at 1020°C for 4 h; (b) air-cooled from solid solution treatment at 1020°C for 4 h.

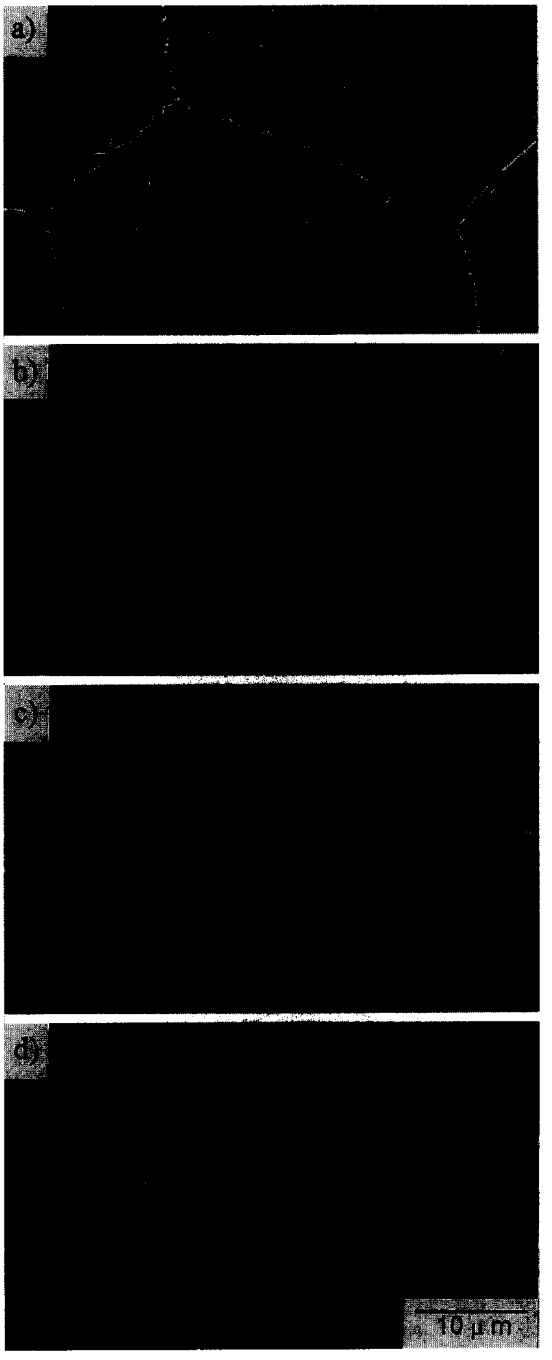

Fig. 2. Microstructures of the material partially solid solution treated at furnace cooling from (a) 900°C; (b) 925°C; (c) 975°C and (d) 1000°C.

All the partially solution treated materials were aged at 725°C for 25 h which produced a homogenous distribution of $\gamma' + \gamma''$ precipitates within the grains. It is seen in Fig. 4 that the size of $\gamma' + \gamma''$ is approximately the same in both the materials with clean grain boundaries and with δ precipitates. The final grain size of all the specimens was about 59 μm.

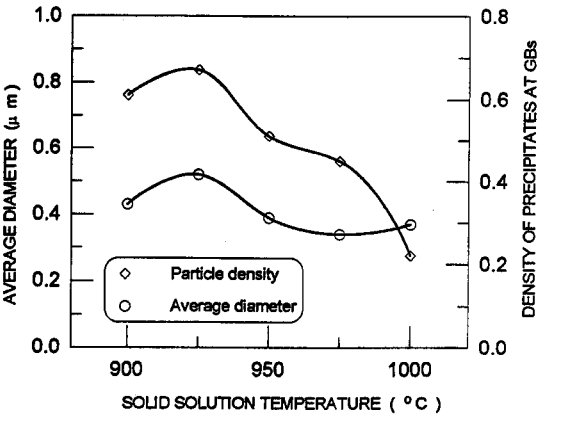

Fig. 3. The effect of partial solid solution temperature on the distribution parameters of δ precipitates at grain boundaries.

3.2. Creep tests

Creep tests on specimens with various densities of grain boundary precipitates were conducted at 795 MPa and 625°C. The creep curves obtained from these tests are given in Figs 5 and 6 which show the variation in creep strain and creep rate with creep time, respectively. It is seen in Fig. 6 that the shape of the creep rate–time curves varies with the amount of precipitates at the grain boundaries. The creep curves of specimens with a lower density of grain boundary precipitates do not show a significant length of steady-state creep stage, although they exhibit a minimum creep rate. An appreciable length of steady-state creep stage, however, can be observed in the material with a value of $\rho \geq 61\%$. The

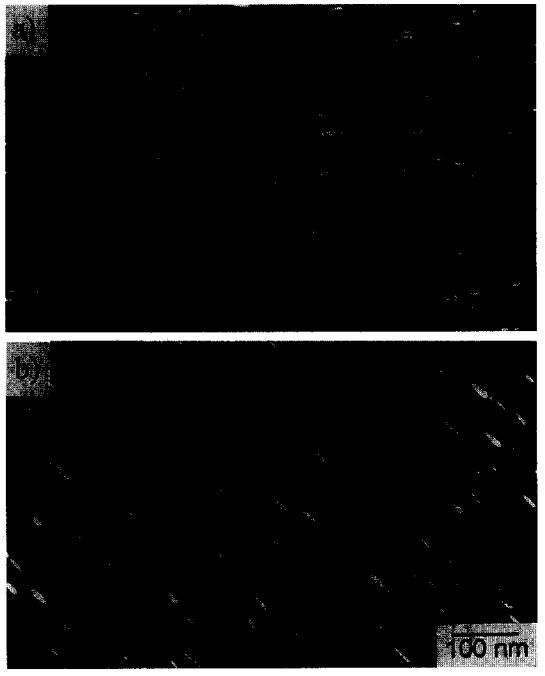

Fig. 4. TEM micrographs showing the distribution of $\gamma' + \gamma''$ in the material with clean grain boundaries (a) and in the material partially solution heat treated at 925°C (b).

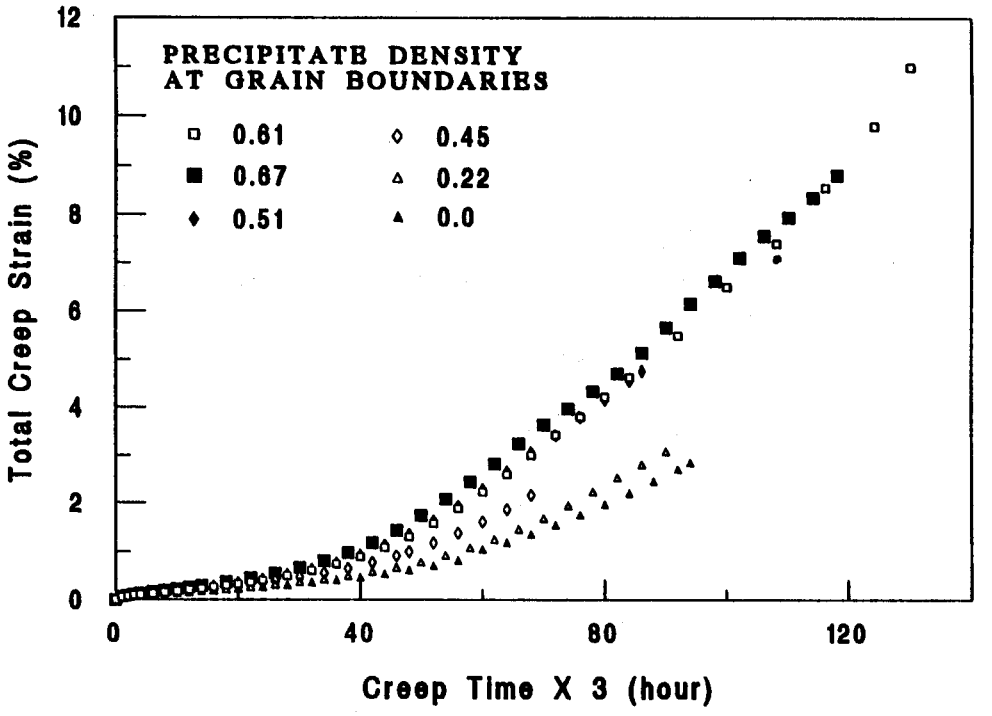

Fig. 5. Creep curves obtained from the test at 625°C and 795 MPa on the material with various precipitate densities at grain boundaries.

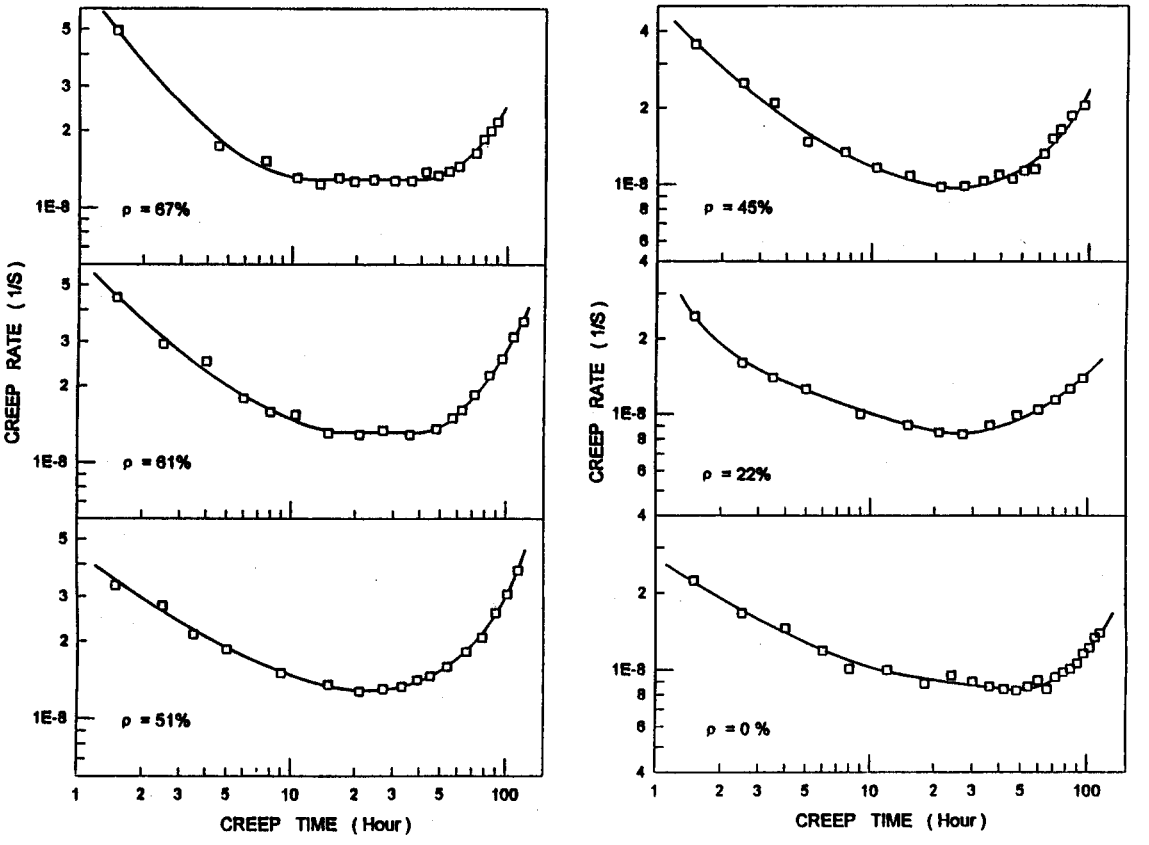

Fig. 6. Creep rate as a function of creep time obtained from the test at 625°C and 795 MPa on the specimens with various precipitate densities at grain boundaries.

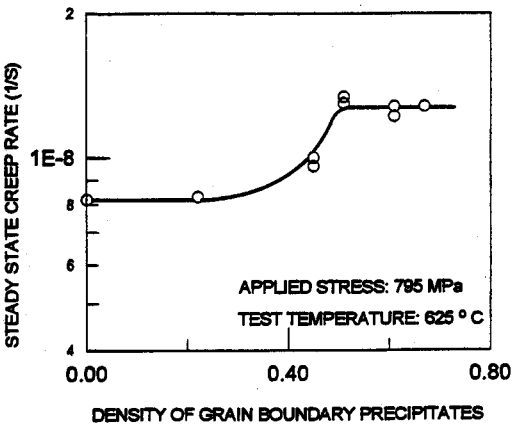

Fig. 7. Variation of steady-state creep rate with the density of precipitates at grain boundaries.

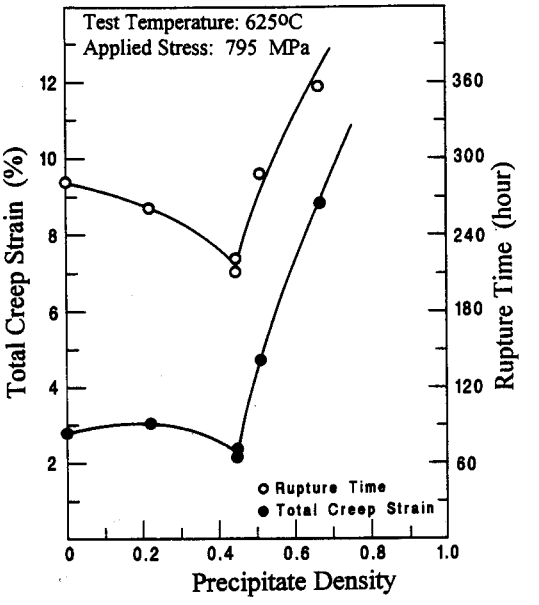

Fig. 8. Dependence of total creep strain and rupture time on precipitate density at grain boundaries.

variation in minimum creep rate (for low GB precipitate density materials) and steady-state creep rate (for high GB precipitate density materials) is shown in Fig. 7. It is seen that the minimum (or steady) creep rates are nearly constant when the density of precipitates at grain boundaries is either high or low. In the intermediate range, however, an increase in creep rate with an increase in density of precipitates at grain boundaries is observed.

The rupture times and the total creep strains of various materials are listed in Table 3. It is seen that the material with a solution treatment at 900°C reaches the highest value in total creep strain and rupture time. The total rupture time and total creep strain are also plotted against the density of precipitates at grain boundaries in Fig. 8. The material partially solution treated at 900°C for 1 h contained coarse precipitates of $\gamma'' + \gamma'$, and its values are, therefore, not included in this figure. It is seen that the total rupture time initially decreases with an increase in density of precipitates at grain boundaries. However, it increases very rapidly when the density of precipitates at grain boundaries is increased to over about 45%. The total creep strain also decreases initially, but then increases rapidly, with an increase in the density of grain boundary precipitates. The minimum in the value of total rupture time and the total creep strain is seen to occur almost at the same density of grain boundary precipitates. The much longer rupture time in the material with high density of precipitates at grain boundaries is also observed when the material is heat treated to produce different grain sizes. The material was first heat treated to produce specimens with three different grain sizes. These were then heat treated to produce materials with clean grain boundaries and with δ precipitates on them. The line density of the precipitates was 67%. The materials were creep tested at a stress of 770 MPa and at a temperature of 625°C. The creep rupture time is shown in Fig. 9. It is seen that all the materials with clean grain boundaries have a smaller creep rupture time compared to those with δ precipitates on them. It is also observed that an increase in grain size reduces the total creep rupture time whether the grain boundaries are clean or decorated with δ precipitates.

3.3. *Fractographic examination*

The fracture surfaces of samples creep deformed to rupture were examined in a SEM to evaluate their fracture behavior. The fracture surfaces of specimens that were partially solution treated at 900, 925, 975 and 1020°C resulting in a value of ρ of 61%, 67%, 45% and 0%, respectively and creep deformed to failure are given in Fig. 10. It is seen that the fracture is intergranular in all cases whether precipitates are present at the grain boundaries or not. For the material with clean grain boundaries, occurrence of deformation on grain boundary facets is not observed, though traces of slip lines in the grain interior are observed [Fig. 10(d)]. When the solid solution treatment temperature is less than 975°C,

Table 3. Summary of creep test results

ρ	0.67	0.61	0.51	0.45	0.22	0
(T)	(925°C)	(900°C)	(950°C)	(975°C)	(1000°C)	(1020°C)
$\dot{\varepsilon}_s$	1.28×10^{-8}	1.21×10^{-8}	1.3×10^{-8}	1.0×10^{-8}	0.83×10^{-8}	0.84×10^{-8}
(1/s)		1.28×10^{-8}	1.33×10^{-8}	9.810^{-8}		
t_{total}	357	390	288	212	261	283
(h)				221		

$\dot{\varepsilon}_s$: steady state or minimum creep rate, t_{total}: rupture time.

heavy deformation is observed at the interfaces of grains where many deformation dimples can be seen [Figs 10(a) and (b)]. Although massive precipitates are present at the grain boundaries in samples which were partially solid solution treated at and above 975°C temperature, no indication of grain boundary deformation is evident.

The polished flat surface of the gage section of failed samples was also examined by SEM to further study the creep fracture behavior and typical micrographs are shown in Fig. 11. It is seen that the wedge-like cracks at triple points of grain boundaries are dominant in the material with clean grain boundaries [Fig. 11(a)]. Some small creep voids on regular grain boundaries are also observed, though they are often associated with intersection site of slip lines and twins and grain boundaries. The wedge cracks at triple points might initiate the fracture in the material with low density of precipitates at grain boundaries. The wedge cracks were seldom observed in materials with high density of precipitates at grain boundaries. Instead, creep cracks are often found on normal grain boundaries.

4. DISCUSSION

4.1. *Effect of strength of grain materials*

The formation of precipitates at grain boundaries will extract some $\gamma' + \gamma''$ forming elements from the grain matrix which should reduce the volume fraction of $\gamma' + \gamma''$ precipitates and hence reduce the strength of grain material. Since the softening of the grain material can assist the relaxation of stress concentration built up around the precipitates, the initiation of creep voids might be delayed and may require a longer time to link-up once initiated. This consideration might be especially significant for the material with a partial solid solution temperature of 900°C at which the coarse $\gamma' + \gamma''$ particles that pre-precipitated during furnace cooling did not dissolve and had grown instead in the grain matrix. This is probably why this material has a much longer rupture time and can also undergo more deformation than the other

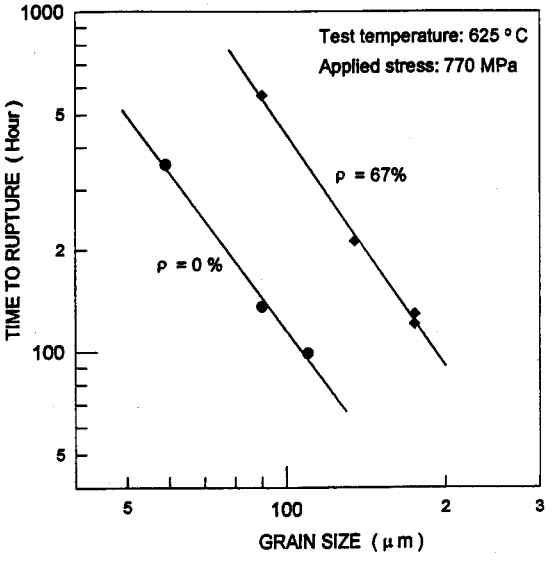

Fig. 9. Variation of time to rupture with grain size.

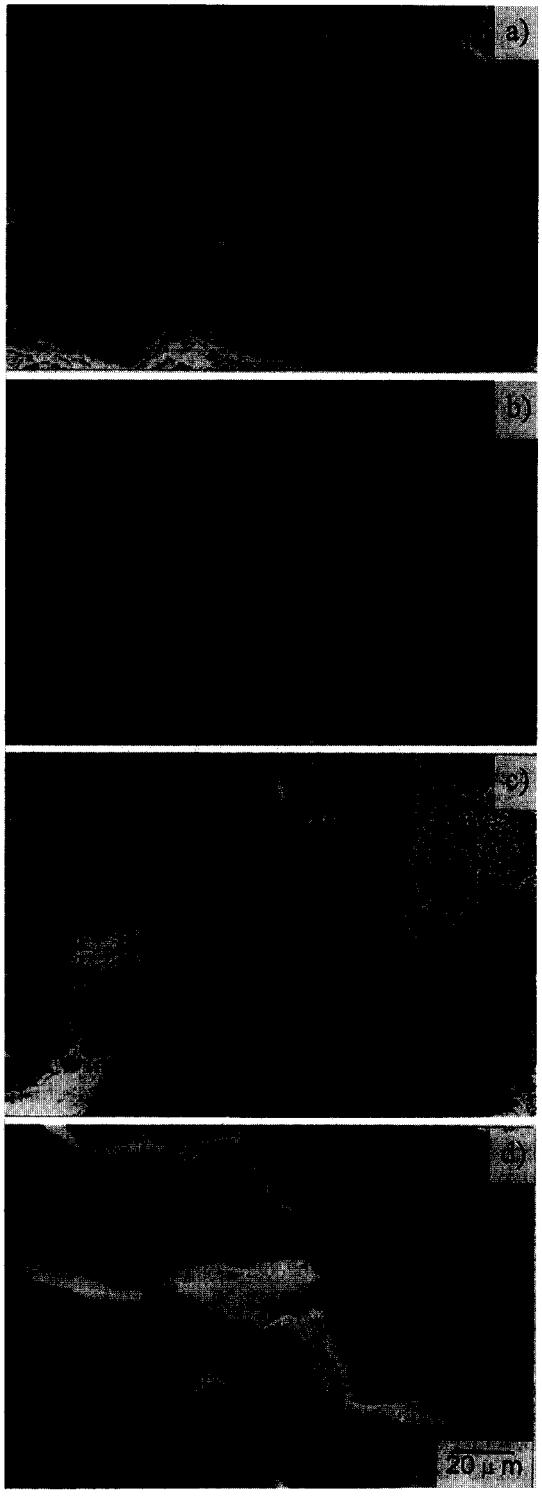

Fig. 10. SEM fractographs of the specimens solid solution treated at (a) 900°C; (b) 925°C; (c) 975°C and (d) 1020°C and creep tested at 625°C and 795 MPa.

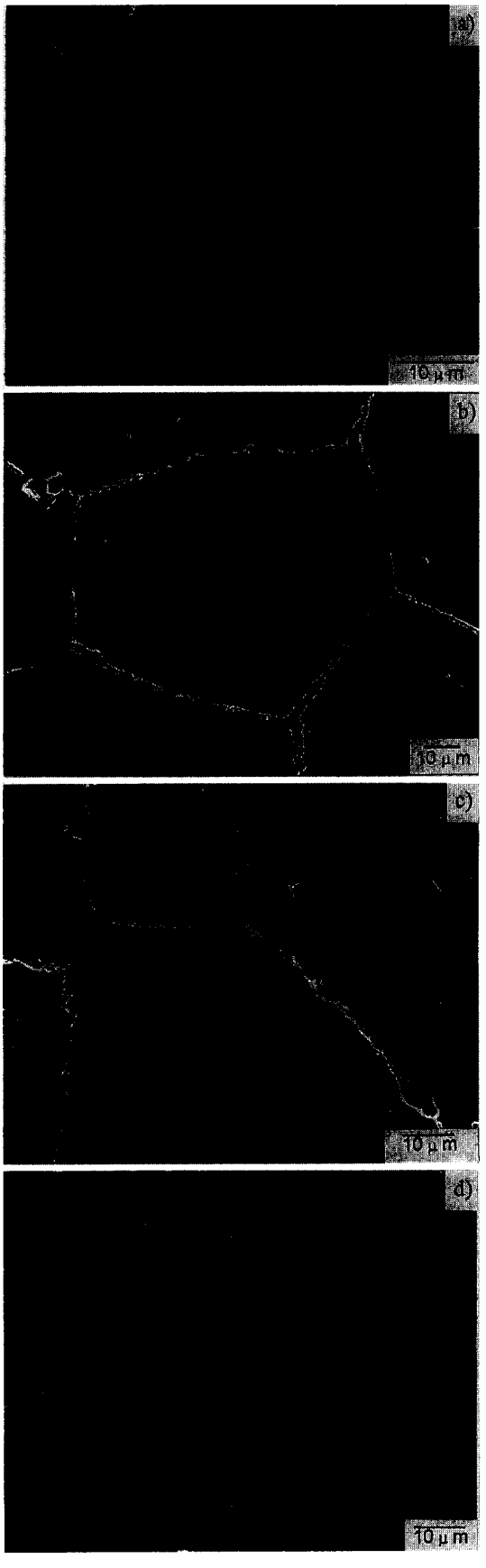

materials that have either higher or lower precipitate density at grain boundaries, as seen in Table 3. In considering the rupture behavior of the material that was partially solution treated at or above 925°C, the decrease in strength of the grain material may not be a key factor in influencing the rupture time and total creep strain. This is because, as observed in Figs 5 and 6, the material with a solid solution temperature of 1000°C exhibits much higher values of rupture time and creep strain than the material treated at 975°C, though the former should have a higher strength grain material due to smaller volume fraction of precipitates formed at the grain boundaries. That is, the grain boundary precipitates may be mostly responsible for the observed fracture behavior, while the weakening effect that occurred in the grain matrix due to the formation of grain boundary precipitates might play only a minor role.

In addition, an interesting observation should be noted here. Although the partial solid solution treatment at 900°C produced coarse intra-granular precipitates, the material with this treatment reached the same steady-state creep rate as obtained in those materials whose grain material strength was much higher. This suggests that the creep deformation resistance of the material is independent of the strength of grain materials. This suggestion is consistent with our previous experimental observations [7], in which the steady-state creep rate was observed to be the same for the materials that were heat treated to possess different grain interior strength.

4.2. *Effect of grain boundary precipitates*

4.2.1. Competition between the formation of wedge-cracks and void link cracks. As observed in Fig. 11, the site where cracks initiated varies with the density (ρ) of grain boundary precipitates. In order to define the conditions under which creep voids might develop at triple points of grain boundaries or around precipitates at the grain boundaries, the concept proposed by Argon *et al.* [9] for characterizing the sliding process of the grain boundary under the influence of grain boundary precipitates might be applicable.

Argon *et al.* [9] considered a set of relatively equiaxed grains containing grain boundary precipitates. They assumed that all boundaries and interphases were incoherent, that grain boundaries slide at the temperature under consideration and that grains had isotopic elastic properties and plastic resistance. On application of load, a series of deformation processes that might occur along a grain boundary were suggested as follows.

Fig. 11. Wedge cracks at the triple points of grain boundaries in the material with clean grain boundaries (a), and with a partial solid solution temperature at 975°C (b). Void-formed cracks in the material solid solution treated at 925°C (c) and 900°C (d).

Table 4. Characterization of grain boundary sliding in the material with grain boundary precipitates

	900°C	925°C	950°C	950°C	1000°C
p (m)	4.3×10^{-7}	5.2×10^{-7}	3.9×10^{-7}	3.4×10^{-7}	3.7×10^{-7}
L (m)	7.1×10^{-7}	7.7×10^{-7}	7.7×10^{-7}	7.5×10^{-7}	16.9×10^{-7}
c	0.606	0.675	0.506	0.453	0.219
$\dot{\varepsilon}_s$ (s^{-1})	1.25×10^{-8}	1.28×10^{-8}	1.32×10^{-8}	9.9×10^{-8}	8.3×10^{-8}
Λ (m)	5.57×10^{-6}	8.52×10^{-6}	2.66×10^{-6}	1.88×10^{-6}	0.3×10^{-6}
t_{BR}(s)	1.92×10^{-7}	1.68×10^{-7}	2.72×10^{-7}	3.03×10^{-7}	12.06×10^{-7}
Δt_{DF} (s)	2.92×10^{-2}	4.16×10^{-2}	2.85×10^{-2}	2.15×10^{-2}	4.91×10^{-2}
$\Delta t'_{DF}$ (s)	5.9	9.7	4.1	2.8	1.6
Δt_{PL} (s)	507.4	1463.9	72.4	29.1	69.8
$\Delta t'_{PL}$ (h)	28.5	94.3	2.86	1.04	0.62

Note: applied stress is 795 MPa; test temperature is 625Δ°C; grain size is 59 μm.

- Within an initial period t_{BR}*, the viscous sliding of all free segments of grain boundaries, not pinned by particles, will relax the shear stress acting across them. This will produce a concentration of stress on all the particles on the sliding grain boundaries, which initiates accelerated power-law creep in the grain matrix around particles and diffusion flow along boundaries with particles. This will tend to reduce the stress concentration.
- Within an additional increment of time Δt_{PL} or Δt_{DF} accelerated power-law creep or diffusional flow around the particles will begin to transfer matter around these grain boundary particles. This will set up an initial steady-state stress concentration around them as overall shear displacements across the boundary begin to occur.
- Such shear displacements along the boundaries, over the particles, will be over a period of $\Delta t'_{PL}$ or $\Delta t'_{DF}$ and will gradually reduce the shear support offered by the grain boundary particles. This will relax even the average shear traction along the entire length of the sliding boundaries, and will build up stress concentrations at triple points.

On the basis of the above hypothesis, it may be suggested that the entire grain boundary may start to slide towards the triple point only when the shear support offered by the grain boundary particles is lost. That is, an incubation period may be needed and can be assumed to be equal to $t_c = t_{BR} + \Delta t_{DF} + \Delta t'_{DF}$ and $t_c = t_{BR} + \Delta t_{PL} + \Delta t'_{PL}$*, both of which correspond to the moment when the concentrated shear stress around particles is relaxed by the diffusion of matter and dislocation creep, respectively. Which of the two processes is dominant can be determined through a comparison of the particle size with a characteristic scaling dimension Λ (for details see Appendix A). When the characteristic scaling dimension Λ is larger than the size of the precipitates, the concentrated stress around the particles will be relaxed by the diffusion of matter around the particles, and by power-law dislocation creep when $\Lambda < p$. The calculation of various characteristic times as well as the characteristic scaling dimension, Λ, is given in Appendix A in detail. Summary of the calculated results is listed in Table 4.

It can be seen from Table 4 that the relaxation of shear stress on the segment of grain boundary between two precipitates is rather rapid. When this relaxation is completed, the shear traction will be concentrated on the particles. The calculated values of Λ, listed in Table 4, indicate that the size of precipitates is less than Λ in all cases except for the material with a second solid solution treatment at 1000°C. In this material, the grain boundaries were decorated with very low density of precipitates. This suggests that the relaxation will take place favorably by matter diffusion around the precipitates. Under this relaxation process, the stress concentrations are generally considered to be too low to initiate cavities around them since, for the initiation of cavities around precipitates, stress concentrations of between 10 and 20 are needed [9]. This suggestion seems to contradict the microstructural observations of crept samples. In a previous investigation [8], the creep voids were observed even in the steady-state stage of creep, and had developed around almost all of the precipitates at grain boundaries in the latter stages of creep. The inconsistency between the results of the calculations and the experimental observations probably can be bridged by the fact that the size of the grain boundary particles is not uniform, but varies over a wide range. As analyzed in detail in Appendix B, grain boundaries in the present material contain two group of precipitates. Precipitates in Group I are very large in size, would be introduced during furnace cooling and would be further coarsened during the subsequent partial solid solution heat treatment, while the precipitates in Group II are small in size and might be produced only in the course of the second solid solution heat treatment. The precipitates in Group II contribute little to the value of the density of precipitates at grain boundaries, however, they substantially decrease the calculated value of average size of grain boundary precipitates. With this consideration, the size of the particles which are effectively pinning a grain boundary is virtually larger than the characteristic scaling dimension, as indicated in Table 4. As a result, relaxation by power-law dislocation creep will become a favorable possibility, so will the development of voids around particles.

The pre-requisite for the formation of a wedge crack is the presence of a concentrated shear stress at

triple points of grain boundaries. In the material where precipitates were present at grain boundaries, this occured only when creep deformation had proceeded over a period of $t_c = t_{BR} + \Delta t_{PL} + \Delta t_{PL}^*$. Therefore, t_c represents the earliest time at which wedge cracks could possibly start to develop at triple points. The variation of t_c with the density of precipitates at grain boundaries is shown in Fig. 12. It is seen that the time t_c increases rapidly with an increase in the density of precipitates at grain boundaries. An additional time over t_c is needed to develop the wedge cracks into a critical size at which rapid propagation can take place.

The initiation of wedge cracks, as indicated in Fig. 12, is unlikely to occur in the material with high density of precipitates at grain boundaries. However, the voids formed around particles can develop into a bigger size and can link up to their neighbors or grow up and eventually become cracks of a size at which rapid crack propagation can occur. The beginning of the tertiary stage should mark the moment when the initiation of these cracks, either of wedge- or void-type has been completed and rapid crack propagation can start. The creep time to the onset of tertiary stage, t_i, is plotted against density of precipitates at grain boundaries in Fig. 13(a). It is seen that with an increase in the precipitate density at grain boundaries, the time required for voids to become unstable cracks will also increase. This might be because the higher the density, the lower the value of the shear stress shared by each precipitate and thus a longer time is needed for the growth of such voids. In contrast to this, the initiation of wedge cracks at triple points seems to be assisted by the presence of precipitates at grain boundaries. This might be due to the extra stress concentration established around the precipitates located at the triple points.

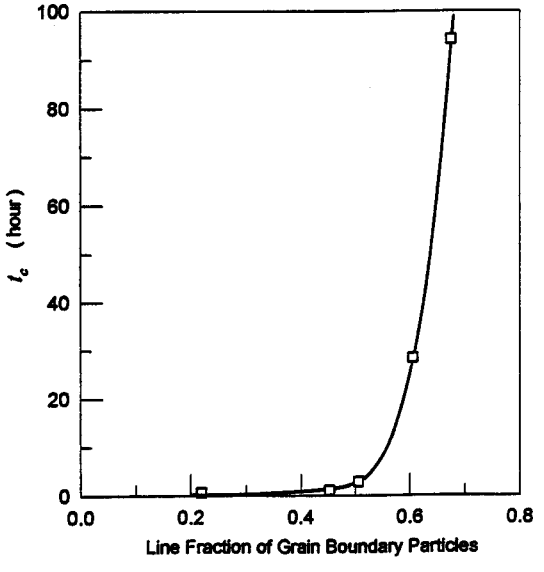

Fig. 12. Variation of δt_c with precipitate density at grain boundaries.

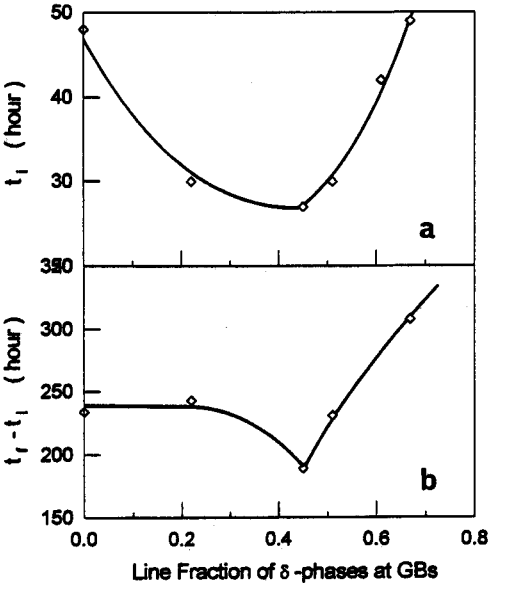

Fig. 13. Variation of time to the tertiary stage and the length of time in tertiary stage with the density of precipitates at grain boundaries.

4.2.2. Final fracture. It has been suggested [11] that the final intergranular cracks during creep deformation can develop by two distinct forms of damage, viz. either by the formation of wedge cracks at the triple points or by the formation of cavity-induced cracks along the grain boundaries. The final fracture often results by the linking of growing cavities and by the extension of wedge cracks, producing grain facet cracks that eventually are bridged together by cavity coalescence along the grain boundaries. The intergranular fracture surfaces after the final fracture were observed to be covered with fine scale dimples corresponding roughly to the mean spacing of particles along the grain boundaries [1]. Such general findings are consistent with those observed in the present investigation in the material with low density of precipitates at grain boundaries. In these materials, both the wedge cracks at triple points and creep cavities associated with the particles along grain boundaries were observed. As a result, extension of wedge cracks was facilitated by the GB particles since voids developed around them. The length of the tertiary stage in this case, therefore, was observed to decrease with an increase in the density of precipitates at the grain boundaries [Fig. 13(b)]. The fracture surface in these materials was also characterized by the decoration of precipitates or cavities with a shape similar to those of the precipitates that have been pulled out from the surface [Fig. 14(b)].

In the material with high density of precipitates at grain boundaries, final fracture was observed to be due to the cracks developed from cavities associated with grain boundary particles. The growth of cavities can occur by absorption of vacancies by cavity surfaces controlled by diffusion [10], by a combination of diffusion and plastic flow [11–14], or by

plastic flow alone [15]. However, in these materials, cracks should develop not simply by coalescence of individual cavities but grain boundary sliding should also play an important role [16]. As shown in Fig. 14(a), the fracture surface in material with a high density of GB precipitates was characterized by large creep cavities which were too large to be the spacing between particles. During sliding, an isolated elliptical cavity may become elongated with sharp tips that resemble cracks [17]. Creep cavities were observed around precipitates at almost all the grain boundaries, an unconstrained growth of cavities should take place in the material with high density of precipitates at grain boundaries [15], and grains would be free to move apart. However, the free sliding of grains may be constrained by the precipitates at grain boundaries [18]. This can be seen from Fig. 15 in which the creep curves representing the materials with high and low density of precipitates at grain boundaries are compared. It is seen that a nearly linear increase in log $\dot{\varepsilon}$ occurs with creep time in the material with $\rho = 0.45$, in which the final fracture was found to be due to the extension of wedge cracks. In the material with $\rho = 0.67$, the tertiary stage is characterized by an initial rapid increase in creep rate followed by several cycles of maxima and minima in creep rate. By comparing these two curves, it is seen that the increase in the length of the tertiary stage when $\rho = 0.67$ is nearly equal to the length of time spent in the creep-rate cycling stage.

It was observed in a previous study [8] that creep cavities often nucleated at the tip of the GB

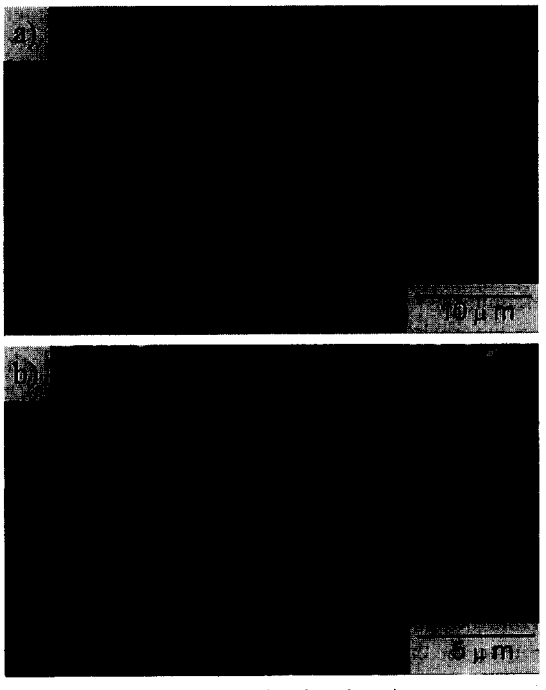

Fig. 14. SEM micrographs showing the microstructures on the intergranular surface of the material with a precipitate density at grain boundaries of 67% (a) and 45% (b), respectively.

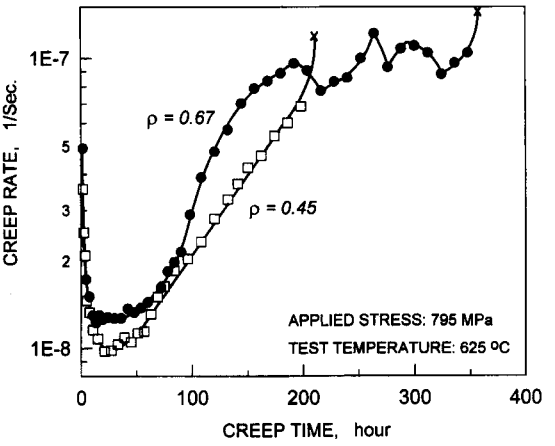

Fig. 15. Creep rate as a function of creep time in the material with a precipitate density at grain boundaries of 67% and 45%, respectively.

precipitates and grew into the segment of grain boundaries free of particles. When sliding occurs, precipitates may tend to shift initially towards the cavity region.This process should be rather easy since little resistance would be encountered inside the cavities, and would correspond to a rapid increase in creep rate during the initial period of the tertiary stage (Fig. 15). If the particles were to fully fill the cavity region, free sliding would be restricted, which would lead to a decrease in creep rate. At the same time, stress concentration may develop again around particles, and a new cycle of nucleation and growth of cavities coupled with grain boundary sliding may start. This cycle would continue until the cracks were large enough to propagate rapidly resulting in the final fracture.

5. CONCLUSIONS

(1) When Inconel 718 is creep deformed at 795 MPa and 625°C, both the total creep strain and rupture time decrease as the density of precipitates at grain boundaries increases to 45%. Above this value of grain boundary precipitate density, total creep strain and rupture time increase with an increase in the density of grain boundary precipitates.

(2) The SEM examination of the fracture surface has shown that wedge cracks form at the triple points when the material has a low precipitate density at grain boundaries. However, creep void-formed cracks on normal boundaries were often observed in the material that had high precipitate density at grain boundaries.

(3) It is suggested that with an increase in the density of precipitates at grain boundaries, the formation of wedge cracks at triple points can be delayed to the stage where creep voids around precipitates at normal grain boundaries are able to grow into unstable cracks. The final fracture in wedge-crack contained materials is suggested to be accelerated by the presence of precipitates since they reduce the grain boundary strength by the introduc-

tion of creep voids around them. However, in the materials containing void-formed cracks, final fracture was observed to be delayed by the presence of a high density of precipitates at grain boundaries. It is suggested that this delay is due to the closure of cavities by the GB precipitates during grain boundary sliding.

Acknowledgements—The authors would like to thank the Natural Sciences and Engineering Research Council of Canada for the financial support and the University of Manitoba for the award of a Graduate Fellowship to W. Chen.

REFERENCES

1. Argon, A. S., in *Recent Advances in Creep and Fracture of Engineering Materials and Structures*. Pineridge Press, Swansea, U.K., 1982, pp. 1–52.
2. Rosler, J. and Evans, A. G., *Mater. Sci. Engng.*, 1992, **A153,** 438.
3. Muzyka, R. and Maniar, G. N., *Metals Engng Quarterly*, 1969, **9,** 23.
4. Koul, A. K., Au, P., Bellinger, N., Thamburaj, R., Wallace, W. and Immarigeon, J.-P., in *Superalloys 1988*. The Metallurgical Society, Warrendale, PA, 1988, pp. 3–12.
5. Camp, E., Turco, C. and Catena, V., *Metall. Sci. Technol., J. Teksid (Italy)*, 1985, **3,** 16.
6. Cadek, J. *Creep in Metallic Materials*, Materials Science Monographs 48. Elsevier, Amsterdam, 1988, pp. 271–343.
7. Chen, W. and Chaturvedi, M. C., *Can. Metall. Quart.*, 1993, **32**(4), 363.
8. Chen, W. and Chaturvedi, M. C., *Mater. Sci. Engng.*, 1997, **A183,** 81.
9. Argon, A. S., Chen, I.-W. and Lau, C.-W., in *Creep-Fatigue-Environment Interactions*, ed. R. M. Delloux and N. S. Stoloff, Conf. Proc. TMS-AIME, Warrendale, PA, 1980, pp. 46–85.
10. Hull, D. and Rimmer, D. E., *Phil. Mag.*, 1959, **4,** 673.
11. Beere, W. and Speight, M. V., *Metals Sci.*, 1978, **12,** 172.
12. Edward, G. H. and Ashby M. F., *Acta metall.*, 1979, **27,** 1505.
13. Needleman, A. and Rice, J. R., *Acta metall.*, 1980, **28,** 1315.
14. Chen, I.-W. and Argon, A. S., *Acta metall.*, 1987, **29,** 1759.
15. Nix, W. D., *Scripta metall.*, 1983, **17,** 1.
16. Evans, H. E., *Phil. Mag.*, 1971, **23,** 1101.
17. Chen, I.-W., *Metall. Trans.*, 1983, **14A,** 2289.
18. Cocks, A. C. F., *Acta metall.*, 1985, **33,** 129.

APPENDIX A: CHARACTERIZATION OF GRAIN BOUNDARY SLIDING PROCESS

The characteristic time described in Section 4.2 was determined by Argon, *et al.* [9] by the following expressions:

$$t_{BR} = B(L/b) \tag{A1}$$

$$\Delta t_{DF} = \frac{B}{8}\left(\frac{p^3}{\Omega}\right) \tag{A2}$$

$$\Delta t_{PL} = B\frac{\Lambda^3}{\Omega} \tag{A3}$$

$$\Delta t'_{DF} = \Delta t_{DF}\left(\frac{d}{L}\right)\frac{\beta(1/4)}{\beta(c)} \tag{A4}$$

$$\Delta t'_{PL} = \Delta t_{PL}\left(\frac{d}{L}\right)\frac{\beta(1/4)}{\beta(c)} \tag{A5}$$

where

$$\beta\left(\frac{p}{L} = c\right) = \cos^{-1}\left\{\frac{1}{\cos\frac{\pi}{2}\left(1 - \frac{p}{L}\right)}\right\} \tag{A6}$$

$$B = \frac{1}{\pi}\left[\frac{kT}{\mu\delta D_B}\right]\beta\left(\frac{p}{L}\right) \tag{A7}$$

$$\Lambda = \left[\left(\frac{p}{L}\right)^{m-1}\frac{\Omega\delta D_B\sigma}{\dot{\varepsilon}kT}\right]^{\frac{1}{3}}. \tag{A8}$$

In these expressions, p is the particle size, L the particle spacing, δ the thickness of the grain boundaries, D_B the grain boundary self-diffusion coefficient, b the length of the Burgers vector, k the Boltzmann's constant, Ω the atomic volume, d the grain size, D_V the volume self-diffusion coefficient, m the stress exponent, and Λ a characteristic scaling dimension. Within a time increment of approximately Δt_{PL} or $\Delta t'_{DF}$, an initial steady state of stress distribution gets established around the grain boundary particles as matter begins to be transported around them between oppositely stressed regions of the particle. This occurs either by diffusional flow along the particle interface or by accelerated power-law creep in the surrounding matrix. The former mechanism dominates for small particles with a size less than the characteristic scaling dimension Λ, while the latter mechanism is dominant for particles much larger than Λ.

Consider the material that was heat treated to have various densities of precipitates at grain boundaries, and was creep tested at 795 MPa and 625°C. The values of various constants of the material are as follows: $G = 64.9 \times 10^9$ Pa, $b = 2.5 \times 10^{-10}$ m, $\Omega = 2.3 \times 10^{-29}$ m^3, $\delta D_B = 2.8 \times 10^{-15}$ exp($-$ 27.4 kcal mol/RT)m^3/s^{-1}, $k = 1.38 \times 10^{-23}$ J/K, $R = 1.987$ cal/(mol K). Based on these data, the characteristic time and scaling dimension Λ for material B were calculated, and are listed in Table 4.

APPENDIX B: DEPENDENCE OF STRESS RELAXATION PROCESS ON THE SIZE OF GB PARTICLES

The calculated values of Λ shown in Table 4 are larger than the average size of the precipitates present at grain boundaries. This suggests, based on the result of Argon *et al.* [9], that the creep voids might be impossible to develop around these grain boundary precipitates. This suggestion contradicts our experimental observations since the voids had been observed around all precipitates at grain boundaries. This contradiction probably can be bridged by the fact that the size of the grain boundary particles is not constant, but varies over a wide range. An example of such a distribution is presented in Fig. B1, in which the material was given a second solid solution treatment at 975°C for 1 h. Figure B1 indicates that the grain boundaries of the material contain two major groups of precipitates: one with a size below the average diameter, another with the size above the average diameter. This broad difference in grain boundary particle size is probably caused by the heat treatment procedures used. The group of precipitates with a larger size would be introduced during furnace cooling and would be further coarsened during the subsequent partial solid

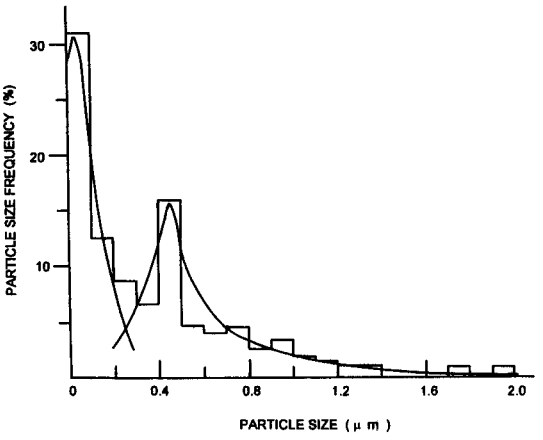

Fig. B1. Size distribution of grain boundary precipitates in the material with a second solid solution treatment at 975°C for 1 h.

solution heat treatment, while the group of precipitates with smaller size might be produced during the course of the second solid solution heat treatment.

If it is considered that the characteristic scaling dimension, Λ, is larger than p, then the time needed for the completion of relaxation of concentration of stress around particles by matter diffusion will vary with the size of the individual particles [refer to equation (A2) in Appendix A]. For example, when the precipitate size is 0.1 μm, Δt_{DF} is about 0.703 s, while when the size is 1.0 μm, Δt_{DF} is 703.1 s. The much sooner completion of relaxation of stress around small particles may make the segment of the grain boundary containing them behave like the part of a grain boundary which is free of precipitates. Therefore, the actual density of grain boundary precipitates—the density of those bigger precipitates that are still undergoing relaxation by matter-diffusion around them, will be decreased. At the same time, the average size of these precipitates will be much bigger than the average size which was calculated with the inclusion of all particles on grain boundaries.

Consider the situation in the material that was given a second solid solution heat treatment at 975°C, and assume that all the particles with a size equal to and below 0.3 μm belong to a group denoted by P_S*, and the rest of them belong to Group P_L*. The fraction of particles in Group P_S was found to be 51.9% of the total precipitates, while the fraction of particles in Group P_L was 48.1% of the total precipitates. The average particle size in Groups P_S and P_L is about 0.11 and 0.653 μm, respectively. The density of precipitates in Group P_L is $0.653 \times 0.481 \div 0.75 = 0.419$. Based on this, the characteristic scaling dimension was calculated to be 0.137 μm. This value of Λ is smaller than the size of the particles in Group P_L. Therefore, diffusion around particles will not be a favored stress relaxation process; instead, power-law creep may take place to relax the concentrations.

These calculations might be helpful in understanding the grain boundary sliding behavior that occurs in the material with precipitates at grain boundaries. Within a very short time of applying stress, relaxation of shear traction can occur on the segments of grain boundaries which are free of precipitates, and concentration of shear traction on particles can be set up. The relaxation of concentration of stress around particles will occur either by mass diffusion around particles or by power-law dislocation creep. The calculations in Table 4 indicate that the diffusion of matter around particles will be favored under the test conditions. However, because of the large differences in the size of precipitates on grain boundaries, the relaxation time will vary significantly with the size of particles on grain boundaries, the small particles will need a much shorter time than bigger particles. The early completion of relaxation of stress around small particles will reduce the number, and also increase the average size of the precipitates that are still undergoing relaxation by the matter diffusion process. This change will cause the characteristic scaling dimension to decrease to a value that might be less than the average size of those grain boundary precipitates around which relaxation by matter diffusion is not completed. As a result, the power-law creep relaxation will prevail over the on-going relaxation by matter-diffusion around the precipitates. Therefore, the initiation of creep voids around particles will become possible. When the stress concentration around the bigger precipitates is completely relaxed, it may also be possible for the stress around smaller particles to undergo the power-law creep relaxation. This is because when the bigger particles loose their pinning to the sliding boundaries, the part of the grain boundaries surrounding them will resemble the segments which were originally free of any precipitates. In this situation, the density of small particles has to be considered, which may cause a characteristic scaling dimension smaller than their average size. When this is the situation, the concentration of stress around precipitate particles can be relaxed by power-law creep deformation. Therefore, it may also be possible to initiate void formation around them. For example, in the case of the material with a solid solution treatment at 975°C, the density of small precipitates is about $0.11 \times 519/0.75 = 0.076$ μm which gives a value of Λ of 0.00015 μm. This value of Λ is much smaller than the average size of small particles (0.11 μm), suggesting that relaxation by power-law can take place.

The proposed mechanism can explain (i) why the creep voids can be initiated around precipitates at grain boundaries even though the matter diffusion around precipitates is a preferred mechanism; and (ii) why creep voids can be observed sooner or later around all the precipitates.